IEEE Access
Multidisciplinary | Rapid Review | Open Access Journal

Received February 17, 2020, accepted April 9, 2020, date of publication April 13, 2020, date of current version April 29, 2020.

Digital Object Identifier 10.1109/ACCESS.2020.2987596

Improving the Positioning Accuracy of Acoustic Emission Events by Optimizing the Sensor Deployment and First Arrival Signal Picking

YANLONG CHEN[1], MINGWEI ZHANG[1], HAOSHUAI WU[1], KAI ZHANG[1], AND DEYU QIAN[2]

[1]State Key Laboratory for Geomechanics and Deep Underground Engineering, China University of Mining and Technology, Xuzhou 221116, China
[2]School of Mines, China University of Mining and Technology, Xuzhou 221116, China

Corresponding author: Mingwei Zhang (mingweizhang@cumt.edu.cn)

This work was supported by the Fundamental Research Funds for the Central Universities under Grant 2019XKQYMS53.

ABSTRACT Acoustic emission (AE) source location is an effective method used to reveal the deformation and damage characteristics of materials. Improving the positioning accuracy of AE events is extremely important for both experimental research and engineering practice. An experiment was performed on a standard rock specimen to investigate the key factors that affect the positioning accuracy of an AE event, such as the computational combinations and spatial layout of the sensors and the picking accuracy of the first arrival signal. The results show that as the number of sensors involved in the positioning calculation increases, both the maximum and average positioning errors clearly decrease, and the positioning accuracy increases. Meanwhile, a better result is achieved when the number of sensors involved in the positioning calculation reaches three-fourths of the total number of monitoring sensors used. Under this condition, both the minimum positioning error and the error dispersion are sufficiently low, and the reliability of the positioning results is greatly improved. Furthermore, when different types of and deviations in the first arrival signal are used for the location calculation of the same AE event, the positioning results are quite different, and large errors are found. Finally, the accurate positioning of an AE event is realized by adjusting the number of sensors and improving the picking accuracy of the first arrival time of the signal. The maximum reduction in the positioning error achieved is 96.62%, and the minimum reduction is 57.61%. Hence, the positioning error decreases significantly. The investigation results can provide an important reference for the precise positioning of AE events involved in experimental research and engineering.

INDEX TERMS Positioning accuracy, acoustic emission, sensor combination and layout, first arrival of signal.

I. INTRODUCTION

As part of the irrecoverable energy dissipation due to the plastic straining of a stressed material, acoustic emission (AE) is highly associated with the material's failure. To date, AE source location has been successfully used for defect localization in many different materials, e.g., crack growth description in concretes or rocks [1]–[5], damage diagnosis for steels [6] and leakage detection from pipes [7]. The main purpose of AE localization is to confirm the spatial positions of internal seismic events induced by fracture initiation and propagation. By observing the abundant real-time AE events during the microcrack fracturing process, the spatial scales and evolution features of the internal microcracks can be confirmed to provide rational, objective evaluation of the material breakage degree [8], [9]. However, the positioning accuracy of AE events is low, and the regularity and reliability are poor in many laboratory experiments and engineering practices [10]–[12]. Generally, a higher positioning accuracy can lead to a deeper understanding of the microcrack evolution in a material. Therefore, the positioning accuracy of AE events has become a notable geophysical parameter that determines the efficiency and reliability of AE monitoring.

Similar to natural earthquakes and mining-induced microseisms, AE phenomena belong to the category of passive seismic sources and have the characteristics of indeterminacy.

The associate editor coordinating the review of this manuscript and approving it for publication was Jenny Mahoney.

How to reduce errors in and improve the positioning accuracy of seismic sources has remained one of the core concerns in the field of passive seismic monitoring [13]–[15]. Most previous studies focused on improving the positioning algorithm of passive seismic sources with the purpose of enhancing the superiority of the algorithm (e.g., accuracy and timeliness). Schumacher *et al*. [16] emphasized that an important step in the quantitative analysis of AE is to estimate the locations of the stress wave sources. These authors introduced a novel holistic framework for the development of a probabilistic source location algorithm using Bayesian analysis with Markov Chain Monte Carlo simulation and posterior probability density functions. Based on the differences among the stress waves measured by six surface-bonded piezoelectric sensors, Ciampa and Meo [17] presented a new in situ structural health monitoring system that is able to identify the location of AE sources caused by low-velocity impacts and determine the group velocity in complex composite structures with unknown lay-up and thickness. The magnitude of the squared continuous wavelet transform modulus was employed for the identification of the arrival time of the flexural Lamb mode. Wang and Ge [18] demonstrated that the source location calculation at a mine site could be improved by a comprehensive source location approach, including digital filtering, reliability analysis, an absolute value-based optimization method and an advanced simplex location algorithm. Nagano *et al*. [19] developed an automatic algorithm of AE source location for AE measurement of subsurface cracks using the triaxial hodogram method. The P-wave arrival time was detected by analyzing the cross-correlation coefficients among three components of AE energy, and the P-wave direction was determined by the least-squares method. Niri and Salamone [20] proposed a probabilistic approach for AE source localization in isotropic plate-like structures based on an extended Kalman filter. Baxter *et al*. [21] described a novel solution for AE source location, ''Delta T'' source location, in complicated geometric structures, using an artificial source to record the differences in the arrival time information from a number of locations. In addition, a 5-step description of the process was provided. Xu *et al*. [22] developed a combined AE location algorithm based on the least-squares algorithm and the Geiger location algorithm and studied the temporal-spatial evolution process of microcracks in similarity experiments of pillar materials with the continuous AE technique. Ciampa and Meo [23] proposed an algorithm for AE source localization based on the differences among stress waves measured by surface-bonded piezoelectric transducers and developed an in situ impact detection monitoring system to identify the real-time AE source location. Kundu [24] presented a noniterative source location algorithm employing four AE sensors and found that the main error in source localization is caused by the arrival time calculation. To reduce the error in the AE signal arrival time calculation, different arrival time calculation methods were compared, and a comprehensive method was proposed. Hensman *et al*. [25] presented a method that ''learns'' the relationship between the time difference of signals and the damage location, using data generated artificially to stimulate AE, and found that the maps learned on a given structure could be effectively generalized to similar structures. Eaton *et al*. [26] carried out a detailed study on the use of a novel mapping technique for AE source localization in fiber-reinforced composite materials. The performance of the approach was assessed with artificial and realistic AE sources. It was found that the positioning accuracy could be considerably improved. Ohtsu [27] performed the moment tensor inversion analysis of AE sources to determine six independent tensor components and elucidate crack types and the orientations of AE sources. It was suggested that tensile cracks were generated first at weak seams and then shear cracking followed along opened joints.

As mentioned above, although efforts have been made to improve positioning algorithms, the spatial location of the passive seismic source cannot be accurately determined. This issue is attributed to the anisotropy of the medium in the seismic wave field. In most situations, the positioning algorithm obtains the most likely position of the seismic source [28], [29]. The difference between the most likely position and the actual position is the main concern. From studies on natural earthquakes, it is observed that the solution of passive seismic spatial positioning can only reduce the error to a certain degree, so optimization of and improvement in the algorithm is required to realize absolute accurate positioning. Hence, it is less significant to consider only the superiority of an algorithm. Under some circumstances, even if a so-called optimized algorithm is adopted, the positioning accuracy is only slightly improved, and no ideal result is achieved. It is difficult to realize the accurate positioning of the absolute spatial location of the seismic source. Furthermore, an optimized positioning algorithm cannot be applied to all types of AE events.

Therefore, it is necessary to determine other factors, in addition to algorithm superiority, that play key roles in improving the positioning accuracy of AE sources. In this paper, AE simulation was performed on a standard limestone specimen, and a multichannel AE monitoring system was utilized. Furthermore, the influencing factors on positioning accuracy were analyzed, such as the computational combinations and spatial layouts of the sensors and the picking accuracy of the first arrival signal. Finally, the positioning error of the simulated AE events is reduced, and the reliability of the positioning is enhanced greatly.

II. POSITIONING ALGORITHM AND EXPERIMENT

A. POSITIONING ALGORITHM

Compared with natural earthquakes and mining-induced microseisms, AE events occur at a smaller scale, in centimeter-scale materials. In view of the generality in AE sources, the positioning algorithm for natural seismic events can also be used for the location determination of AE events.

In a Cartesian coordinate system, the distance (D_n) between the AE sensors and a specific AE event can be determined as follows [24], [30]:

$$D_n = \sqrt{(x_n - x_0)^2 + (y_n - y_0)^2 + (z_n - z_0)^2} = v \times (t_n - t_0) \quad (1)$$

where x_n, y_n, z_n, and $t_n (n = 1, 2, 3 \cdots)$ are the predetermined coordinates of the n-th AE sensor and the arrival time detected by each sensor, respectively; x_0, y_0, and z_0 are the coordinates of the AE event source location; v is the wave velocity; and t_0 is the origin time of the AE source.

According to Eq. (1), the objective function can be established:

$$f(x_0, y_0, z_0, t_0) = \sum_{n=1}^{N} \left[t_n - \frac{1}{v}\sqrt{(x_n - x_0)^2 + (y_n - y_0)^2 + (z_n - z_0)^2} - t_0 \right]^2 \quad (2)$$

where N is the number of the sensors.

Generally, the wave velocity is assumed to be constant, so there are only four unknowns in Eq. (2), including the spatial coordinates of the AE event source and origin time of the AE source. By taking each sensor datum to Eq. (2), an equation can be obtained; four sensors correspond to four equations, which constitute a set of nonlinear equations. Therefore, a four-sensor array would be able to localize one AE event based on the time difference of arrival (TDOA) among sensors [24], [31], [32]. In this study, twelve sensors are arranged to eliminate potential errors.

According to Eq. (2), the closer the calculated position is to the actual position of the AE source, the smaller the result of the objective function. Hence, the process of inverse positioning of the AE source is the process of calculating the minimum value of the objective function. In Eq. (2), the positions of the AE sensors can be determined during the experimental setup. Therefore, reliable signal source location requires accurate determination of the arrival times picked by each sensor.

Therefore, it can be seen that the computational combinations and spatial layouts of sensors and the pickup accuracy of the signal first arrival will obviously affect the location result. An experiment will be implemented to investigate these factors for affecting the positioning accuracy of AE event.

B. EXPERIMENT

To analyze the influence of key factors other than the algorithm on the accuracy of AE source positioning, the artificial shock mode was applied in this study to generate the simulated AE sources. Since the practical spatial position of the impact point is known, it is convenient to compare it with the calculated position. In the experiment, the AE signals detected by the sensors were digitalized continuously with a sampling rate of 1250k samples per second through a high-speed data logger called SEMOS-lab (12 channels). The sensors were closely adhered to the surface of the standard cylindrical rock specimen with a diameter of 50 mm and height of 100 mm. The twelve AE sensors (Sen1 to Sen12) were orthogonally arranged in 4 columns and 3 rows at a spacing of 30 mm and were closely coupled with the rock specimen to synchronously and continuously monitor the seismic wave propagation after the artificial excitation. Meanwhile, one iron nail (In) and one iron rod (Ir), with black ink on their cusps, were taken and thrown from different directions and heights to generate 8 random active shot points (In1 to In4, Ir1 to Ir4) on the upper surface of the rock specimen. Instantaneous shock signals generated from the artificial excitation were recorded by the AE sensors in real time. With the black ink, the iron nail and iron rod accurately marked the striking positions, and the actual positions of the simulated AE event sources can be observed. This experimental scheme has the superiority that the actual spatial positions of the simulated AE events can be compared directly with those calculated from the positioning algorithm. This is convenient for verifying the reliability of the results and evaluating the positioning accuracy. The experimental devices and scheme are shown in Fig. 1. By considering the geometric center of the rock specimen as the origin of the Cartesian coordinate system, the spatial coordinates of the twelve AE sensors are summarized in Table 1.

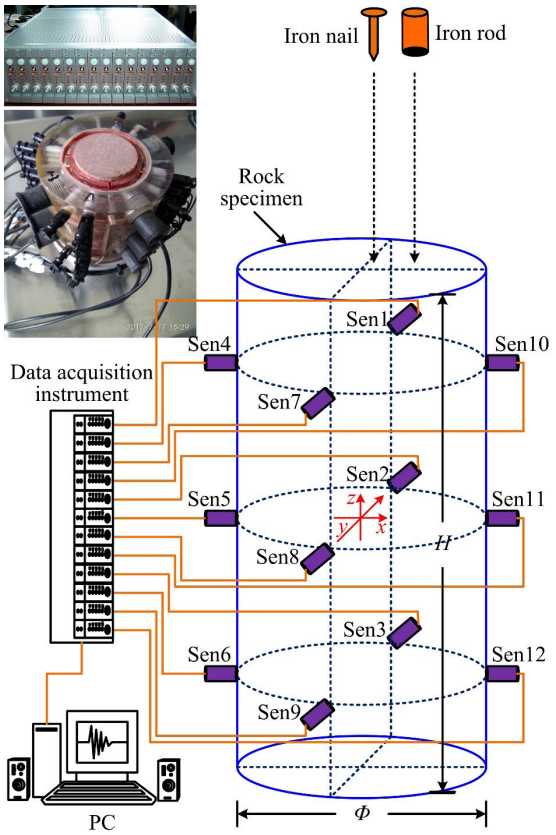

FIGURE 1. Experimental devices and schemes.

TABLE 1. Spatial coordinates of the AE sensors.

AE sensors index		Sen1	Sen2	Sen3	Sen4	Sen5	Sen6	Sen7	Sen8	Sen9	Sen10	Sen11	Sen12
Spatial coordinates (mm)	X	0	0	0	-25	-25	-25	0	0	0	25	25	25
	Y	25	25	25	0	0	0	-25	-25	-25	0	0	0
	Z	30	0	-30	30	0	-30	30	0	-30	30	0	-30

TABLE 2. Spatial locations of eight simulated AE events.

Spatial positions	AE events							
	In1	In2	In3	In4	Ir1	Ir2	Ir3	Ir4
X (mm)	-1.7514	0.6963	2.0061	0.5448	-10.7353	10.4304	2.5034	8.6388
Y (mm)	2.9593	10.6973	4.5361	0.4094	-4.3573	-0.2301	-2.4937	-7.2847
Z (mm)	50	50	50	50	50	50	50	50

Note: In indicates Iron nail; Ir indicates Iron rod.

TABLE 3. First arrival time of eight AE events.

	Channels	AE events							
		In1	In2	In3	In4	Ir1	Ir2	Ir3	Ir4
First arrival time (μs)	1	4340.8	3140.8	4227.2	4552.8	4519.2	3292.8	4040.8	1080.0
	2	4347.2	3144.8	4233.6	4559.2	4525.6	3296.8	4047.2	1087.2
	3	4354.4	3151.2	4240.8	4567.2	4533.6	3303.2	4056.0	1093.6
	4	4342.4	3140.0	4228.8	4555.2	4522.4	3293.6	4041.6	1082.4
	5	4348.8	3146.4	4235.2	4561.6	4528.8	3298.4	4048.8	1088.0
	6	4358.4	3152.8	4242.4	4568.0	4533.6	3304.8	4053.6	1093.6
	7	4341.6	3136.8	4225.6	4553.6	4520.8	3291.2	4042.4	1083.2
	8	4347.2	3143.2	4232.8	4559.2	4526.4	3296.8	4048.0	1088.8
	9	4355.2	3150.4	4240.0	4567.2	4532.8	3303.2	4054.4	1094.4
	10	4340.0	3138.4	4227.2	4553.6	4519.2	3292.8	4042.4	1082.4
	11	4349.6	3145.6	4233.6	4560.8	4526.4	3298.4	4048.0	1088.0
	12	4356.8	3149.6	4241.6	4565.6	4532.0	3303.2	4053.6	1092.8

Note: In indicates Iron nail; Ir indicates Iron rod.

III. RESULTS

A. SPATIAL COORDINATES OF THE AE SOURCES

Based on the experiment, the locations of eight AE events are recorded (Fig. 2). The spatial positions of these AE events are obtained by microscopic image analysis (Table 2).

B. FIRST ARRIVAL TIME PICKING OF AE SIGNAL

A group of seismic signals (In2) are obtained from the experiment and are given in Fig. 3. Based on the relative rules of arrival time picking, the first arrivals of these recorded seismic waves in every channel are picked from the take-off points of the P waves (Table 3).

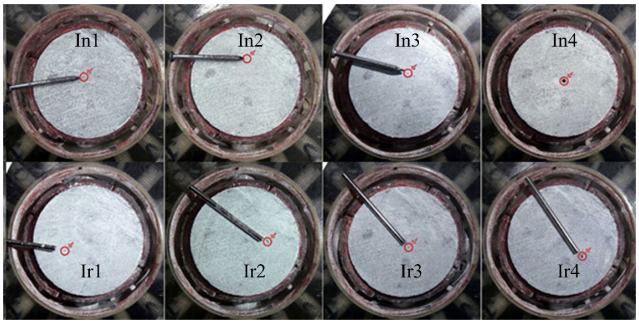

FIGURE 2. Position of impact points induced from the freely falling iron nail or iron rod.

C. POSITIONING CALCULATION RESULTS OF AE EVENTS

When the computational combinations are twelve, the type of first arrival of signal adopts take-off point, deviation of first arrival uses zero point, the locations and positioning errors of these eight simulated AE events are determined as shown in Figs. 4 and 5.

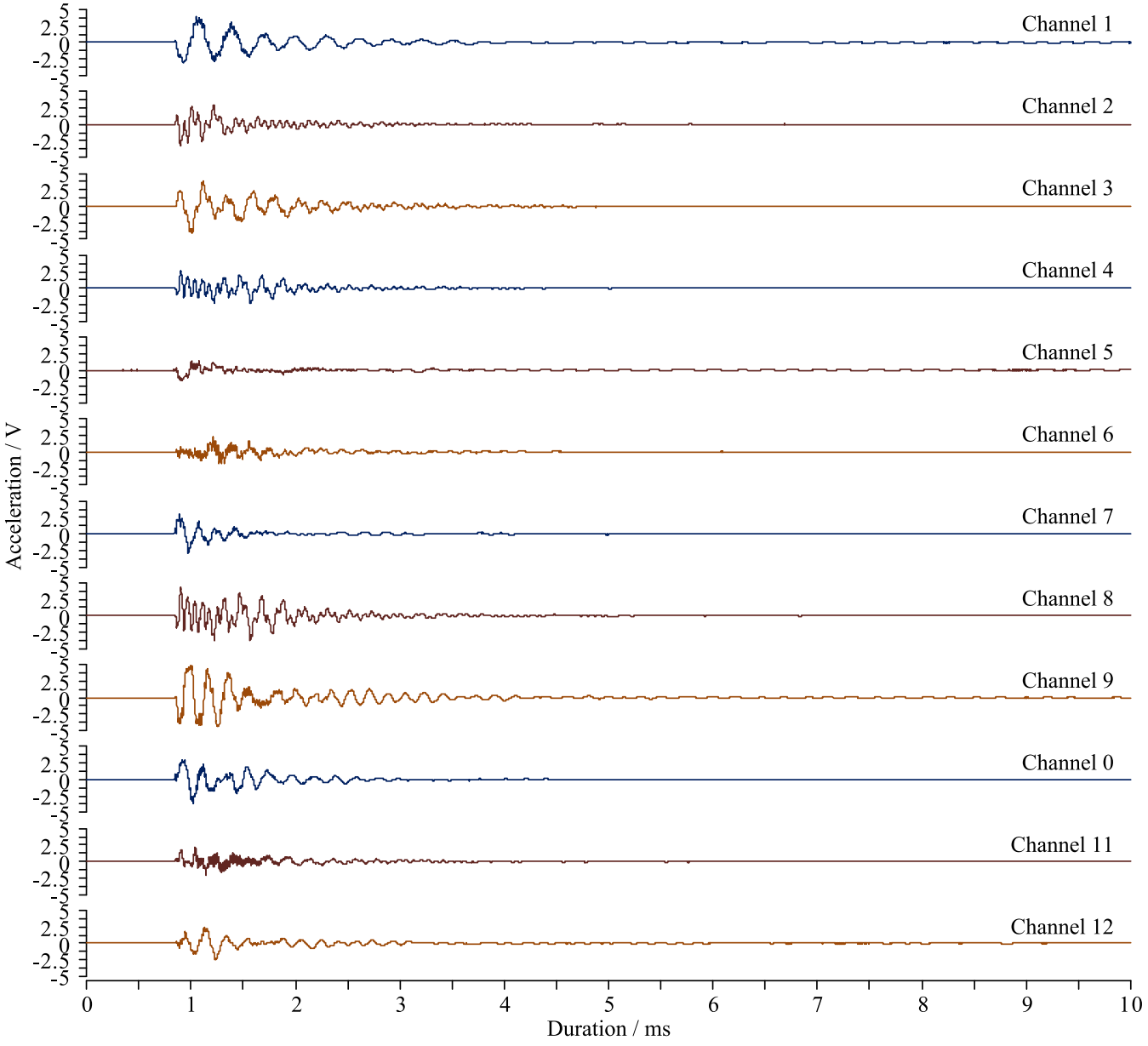

FIGURE 3. Signal group of an AE event (In2).

Under the same experimental conditions, the error between the calculated position and the actual position of the eight simulated AE events is significant even if the same algorithm is used for positioning calculation and only the shock points are changed. The maximum error reaches 12.6410 mm (In2 event), while the minimum error is 1.0848 mm (Ir4 event). This finding indicates that the accuracy of the positioning is not completely dependent on the algorithms but is also highly dependent on other factors. The parameters involved in the positioning calculation mainly include the spatial coordinates of the sensors and the first arrivals of the P-waves. The sensor coordinates are fixed, and the sensors involved in the source location determination are selected. The first arrival times of the signals are artificially marked and selected. These factors are significantly affected by a few extrinsic factors, such as the noise, artificial judgment, sensor number and rock physical properties. The fact that the seismic source positioning is inaccurate does not necessarily result from an unreliable algorithm. In some situations, the inaccuracy is caused by the poor picking accuracy of the first arrival or the unreasonable selection of a senor. Changes in any factor will cause positioning errors to varying degrees and hence affect the reliability of seismic positioning calculations. Among the eight simulated AE events, In2 has the maximum positioning error. Therefore, to analyze the positioning error induced by multiple factors, the In2 event is taken as an example in

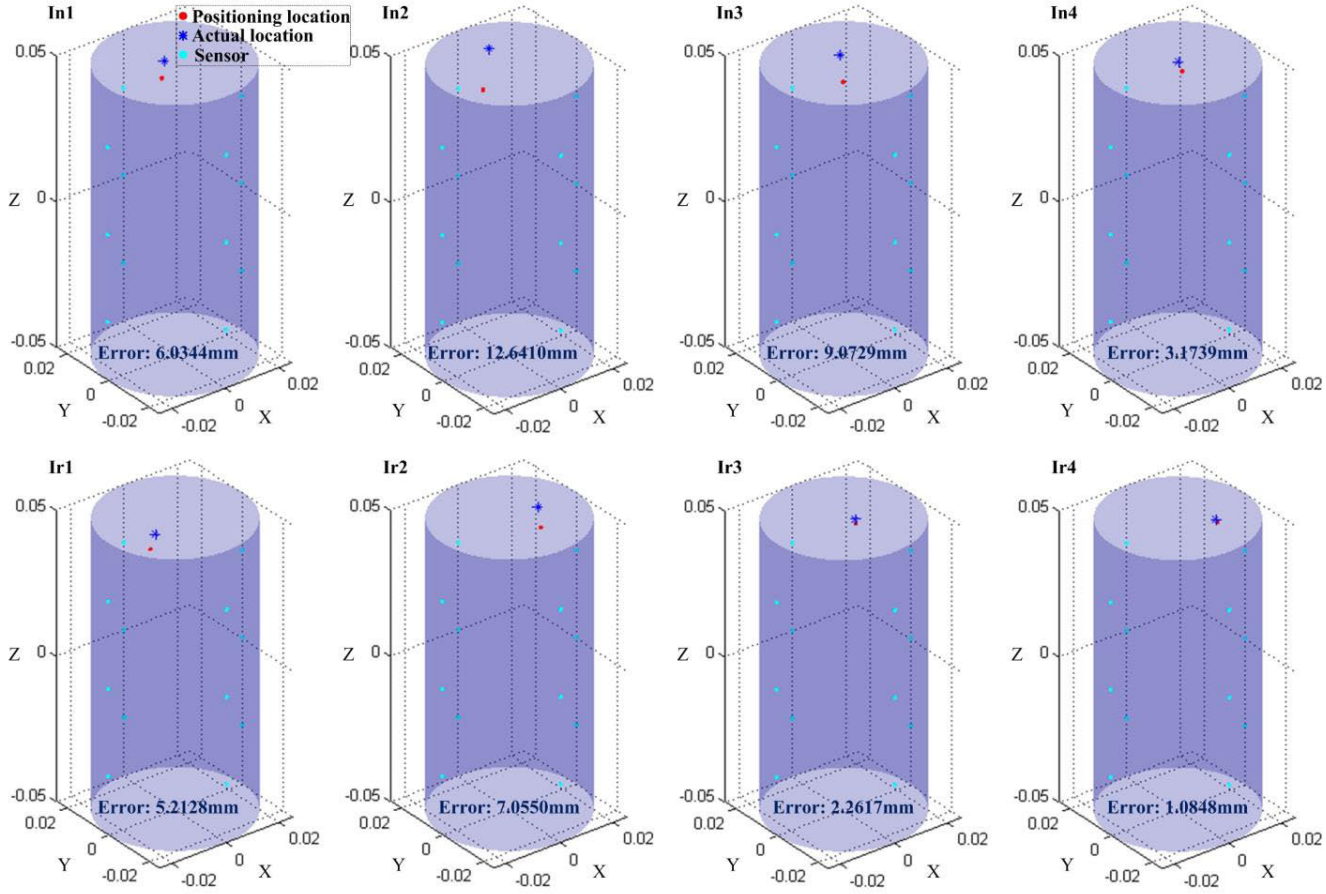

FIGURE 4. Comparison between the calculated positions and actual positions of the simulated AE events.

this study. The same positioning algorithm is used, and the influences of computational combinations and spatial layout of the sensors, the first arrival time picking accuracy will be discussed.

IV. DISCUSSION

For passive seismic positioning, the accuracy of the calculation result depends on the positioning error. Error between the calculated position and the actual position always exists. Factors influencing the positioning error can be divided into two kinds: uncontrollable and controllable. Uncontrollable factors mainly include the positioning algorithm and material anisotropy, while controllable factors vary (e.g., the computational combination, sensor spatial layout, signal first arrival picking and sampling frequency). In the following context, taking the case of the In2 seismic source as an example, the influences of controllable factors on positioning accuracy will be analyzed.

A. IMPACT OF THE COMPUTATIONAL COMBINATIONS AND SPATIAL LAYOUTS OF SENSORS

Based on the Geiger ray positioning principle, the number of sensors used for the determination of the absolute source location should be no less than four. The total number of sensors in this experiment is twelve. Table 4 provides the quantitative positioning results of the In2 seismic source in various situations when different combinations of sensors are used for positioning calculation. When the number of sensors

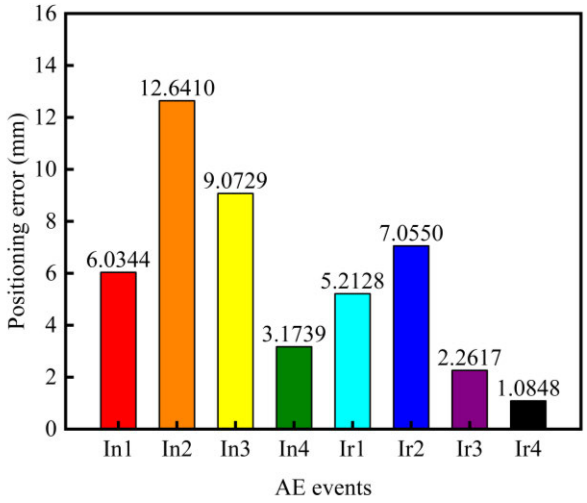

FIGURE 5. The positioning error of different AE events.

TABLE 4. The positioning error of the In2 seismic source under the different computational combinations of sensors.

Number of sensors	4	5	6	7	8	9	10	11	12
Number of results	495	792	924	792	495	220	66	12	1
Max. value (mm)	100.472	69.161	64.910	62.777	62.8	37.1	29.6	20.9	12.641
Min. value (mm)	0.429	0.429	0.429	0.429	0.429	0.429	2.139	5.704	12.641
Avg. value (mm)	24.328	24.200	19.370	16.642	15.267	14.455	13.833	13.030	12.641

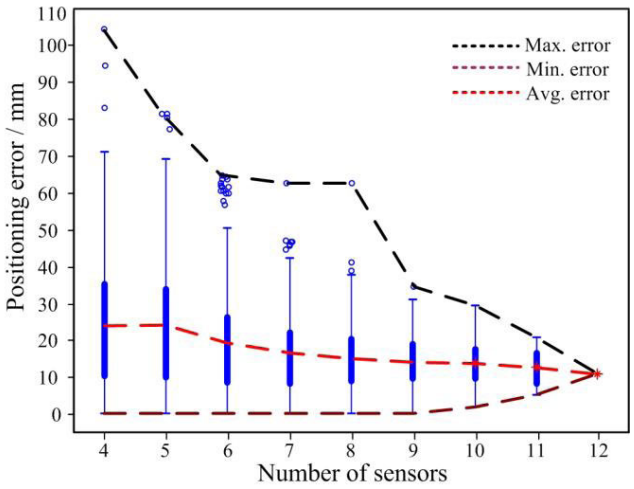

FIGURE 6. The positioning error of the In2 seismic source with the increase in the number of sensors.

involved in the positioning calculation ranges from four to twelve, there are 3797 positioning results in total, as shown in Table 4. According to Table 4, a statistical analysis is performed on every quantitative combination, and the changes in positioning error with the increase in the number of sensors are presented in Fig. 6, including the maximum, minimum and average values of the positioning error.

Fig. 6 shows that with the increase in the number of sensors involved in the positioning calculation, the maximum and average values of the positioning errors gradually decrease. When the number of sensors increases from four to twelve, the maximum positioning error changes from 100.472 mm (when Sen1, Sen4, Sen7 and Sen10 are employed) to 12.641 mm (when Sen1 to Sen12 are employed), which is a reduction of 60%, and the average positioning error changes from 24.328 mm to 12.641 mm, which is a reduction of 48%. It is indicated that the reliability of the positioning accuracy usually strengthens if more channels are used in the calculation. Therefore, more sensors are suggested when positioning passive seismic sources. This approach does not necessarily decrease the specific positioning error but often plays a key role in reducing the error in most situations.

Moreover, the minimum positioning error is found according to different combinations of sensors. When the number of sensors ranges from four to nine, the minimum positioning error is 0.429 mm (the applied minimum grid scale is 1 mm). In these cases, the utilized sensors are Sen2, Sen4, Sen8, and Sen10; Sen2, Sen4, Sen8, Sen9 and Sen10; Sen1, Sen2, Sen4, Sen7, Sen9 and Sen10; Sen1, Sen2, Sen4, Sen7, Sen8, Sen9 and Sen10; Sen1, Sen2, Sen4, Sen5, Sen7, Sen9, Sen10 and Sen11; and Sen1, Sen2, Sen4, Sen5, Sen7, Sen8, Sen9, Sen10 and Sen11. However, the minimum positioning error increases gradually to 2.139 mm (Sen1, Sen2, Sen4, Sen5, Sen7, Sen9, Sen10, Sen11 and Sen12), 5.704 mm (Sen1, Sen2, Sen3, Sen4, Sen5, Sen 6, Sen7, Sen9, Sen10, Sen11 and Sen12) and 12.641 mm (Sen1, Sen2, Sen3, Sen4, Sen5, Sen 6, Sen7, Sen8, Sen9, Sen10, Sen11 and Sen12) when the numbers of sensors are ten, eleven and twelve, respectively. The minimum positioning error is almost the same (0.429 mm) when the number of sensors ranges from four to nine and then increases by 30 times (from 0.429 mm t0 12.641 mm) when the number of sensors ranges from nine to twelve.

Hence, a better result is achieved when the number of sensors involved in the positioning calculation is nine, accounting for three-fourths of the total number of monitoring sensors. Under this condition, both the minimum positioning error and the error dispersion are sufficiently low, and the reliability of the positioning results is greatly improved.

In addition, the spatial layout of the sensors is also a key factor affecting the reliability and effectiveness of AE event positioning. Based on the spatial layout of the AE sensors, the space in which the AE events may be localized is divided into two types. One region is the largest internal space covered by all sensors, which is called the sensor-controlled region. The other region is the space outside of the sensor-controlled region. The positioning accuracy is generally higher if the actual seismic source is in the sensor-controlled region. When the source locations of the AE events are calculated, it is often found that the variation in the source error in the three-dimensional space is inconsistent.

In this research, the deviation in the positioning in the X and Y directions is limited but becomes obvious in the Z direction. This phenomenon is closely related to the spatial layout of the AE sensors in the experiment. Because the dimensions of the rock specimen are 50 mm in diameter and 100 mm in height, the spatial density and control range of the sensors in the X and Y directions are greater than those in the Z direction in this study, which easily ensures the positioning accuracy in the X and Y directions with the sensors in different locations. The extensions of the sensors in the Z direction are significantly smaller than those in the other two directions, which leads to weaker controllability of the sensors in this direction and higher deviation in the

TABLE 5. Comparisons of the positioning errors of simulated AE events using the different types of first arrivals (deviation in first arrival: 0 point).

Types of first arrival		Take-off point	First crest	First trough	First zero creep	Cross-correlation point	Maximum energy point
Positioning error (mm)	In1	6.0344	7.9523	11.4101	10.5455	5.2508	9.7511
	In2	12.6410	11.3713	15.2645	17.5449	8.2582	13.4619
	In3	9.0729	8.1722	10.1937	9.9078	11.9760	10.4488
	In4	3.1739	4.2279	5.2316	3.3801	2.5950	4.4918
	Ir1	5.2128	7.8530	5.4269	3.7094	6.9610	7.7975
	Ir2	7.0550	5.1786	8.2787	8.2774	8.7157	6.9611
	Ir3	2.2617	3.8242	2.1077	4.2938	2.2684	1.1847
	Ir4	1.0848	2.7550	4.0621	1.7475	3.5853	4.0187

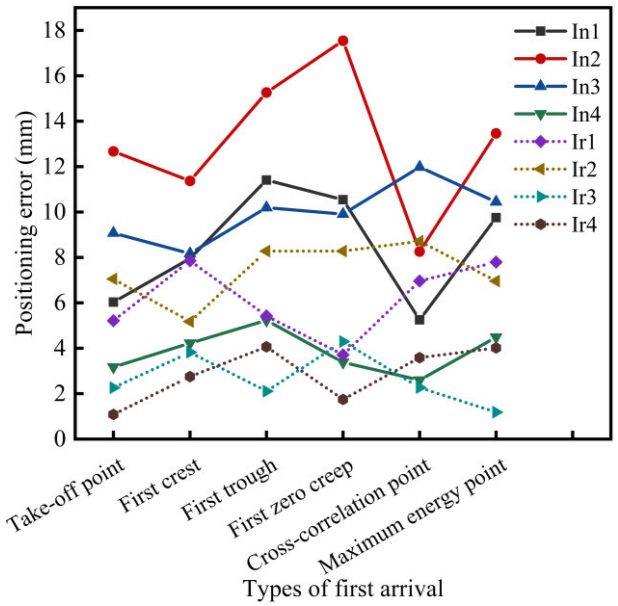

FIGURE 7. The positioning error of different AE events under the different types of first arrivals (deviation in first arrival: 0 point).

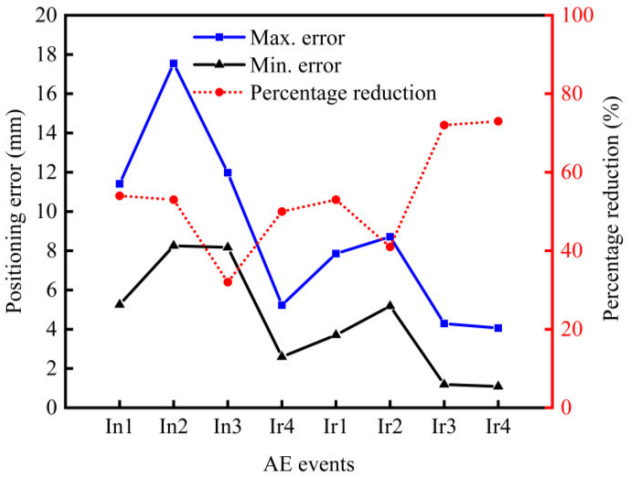

FIGURE 8. The maximum and minimum positioning error and their percentage reduction for different AE events considering the different types of first arrivals (deviation in first arrival: 0 point).

positioning. Therefore, it is quite significant to optimize the spatial layout of the sensors in AE source positioning, and the sensors should be uniformly arranged as possible around the seismic source.

B. IMPACT OF THE PICKING ACCURACY OF THE FIRST ARRIVAL OF THE AE SIGNAL

The first arrival of the seismic wave signal is one of the key factors that affect the positioning reliability of AE events. The accuracy of the AE source positioning is closely related to the types and deviation in the picking of the first arrival. The types of first arrival usually include the take-off point, the first crest, the first trough, the first zero creep, the cross-correlation point and the maximum energy point. On the other hand, the deviation in the picking of the first arrival is sensitive to the sampling interval.

For the eight simulated AE events presented in the study, if a consistent algorithm and related parameters are considered, the spatial locations of the shock points are repositioned when the first arrivals of different types and the deviations in every signal channel are chosen for calculation. Table 5 and Fig. 7 show the positioning errors of simulated AE events using the different types of the first arrivals considering that the deviation in the first arrival is the zero point. Table 6 and Fig. 8 present the maximum and minimum positioning errors and their percentage reduction from the maximum error to minimum error for AE events considering the different types of first arrivals.

It is seen that under different types of first arrivals for the same seismic event, the positioning results are quite different, and large errors are observed. Surprisingly, the greatest reduction percentage from the maximum error to minimum error can reach 73% for the same AE event (case Ir4), and the smallest reduction percentage is 32% (case In3).

Moreover, Table 7 and Fig. 9 show the positioning error of simulated AE events using the different deviations in the first arrival signal under the take-off point type of first arrival). Table 8 and Fig. 10 illustrate the maximum and minimum positioning errors and their percentage reduction from the maximum error to minimum error for AE events under the different deviations in the first arrival signal. It is found

TABLE 6. The maximum and minimum positioning errors and their percentage reduction for different AE events considering the different types of first arrivals (deviation in first arrival: 0 point).

AE events		In1	In2	In3	In4	Ir1	Ir2	Ir3	Ir4
Positioning error (mm)	Max. error (mm)	11.4101	17.5449	11.9760	5.2316	7.8530	8.7157	4.2938	4.0621
	Min. error (mm)	5.2508	8.2582	8.1722	2.5950	3.7094	5.1786	1.1847	1.0848
	Percentage reduction (%)	54	53	32	50	53	41	72	73

TABLE 7. Comparisons of the positioning errors of simulated AE events using the different deviations in the first arrivals (type of first arrival: take-off point).

Deviations of first arrival		Sampling interval				
		-2 points	-1 point	0 point	1 point	2 points
Positioning error (mm)	In1	6.3801	8.3985	6.0344	5.8131	9.7987
	In2	12.9476	9.3851	12.6410	12.2081	13.5779
	In3	10.7563	9.5298	9.0729	11.796	7.7465
	In4	7.4379	9.3292	3.1739	9.2910	4.0341
	Ir1	5.7772	4.1442	5.2128	2.1692	6.1194
	Ir2	11.0714	11.2036	7.0550	8.7499	10.0802
	Ir3	5.7568	2.4596	2.2617	6.8867	7.7334
	Ir4	3.0608	8.4324	1.0848	5.8451	9.9652

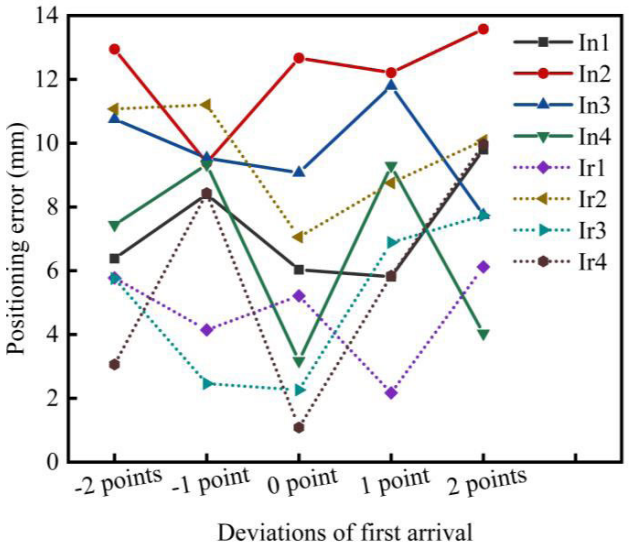

FIGURE 9. The positioning error of different AE events under the different deviations of the first arrival signal (type of first arrival: take-off point).

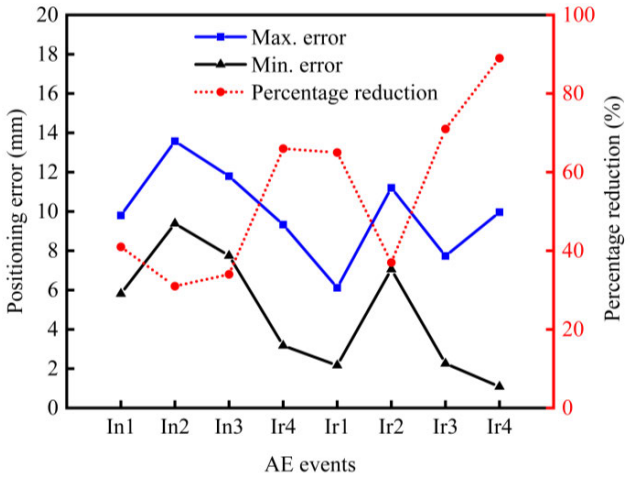

FIGURE 10. The maximum and minimum positioning error and their percentage reduction for different AE events considering the different deviations in the first arrival signal (type of first arrival: take-off point).

that under different deviations in the first arrival signal, the positioning results are also extremely different. The greatest reduction prcentage from the maximum error to minimum error is 89% for the same AE event (case Ir4), and the smallest reduction percentage is 32% (case In2).

As mentioned above, when different types of and deviations in the first arrival signal are used for the source calculation of the same seismic event, the positioning results are quite different, and large errors are found. Taking the case In2 seismic source as an example, the positioning error reaches the minimum (8.2582 mm) if the first arrival deviation has no sampling interval and the cross-correlation point is used. However, the error increases by 2.12 times (17.5449 mm) when the first zero creep is used. The positioning error is minimal (9.3851 mm) under the condition that both the take-off point and the sampling interval (−1 point) are applied, and the error increases by 1.45 times (13.5779 mm) as the sampling interval increases to 2 points.

Picking of the first arrival of the AE seismic waves seems simple but is quite difficult if high precision is needed. The local wave phase and morphology of every signal are different. It is unreliable to use uniform rules to determine the first arrival signal, especially without considering the effect of superimposition and dissimilation of multiple seismic wave phases. Therefore, accurate and reliable picking of the first arrival signal is an important prerequisite

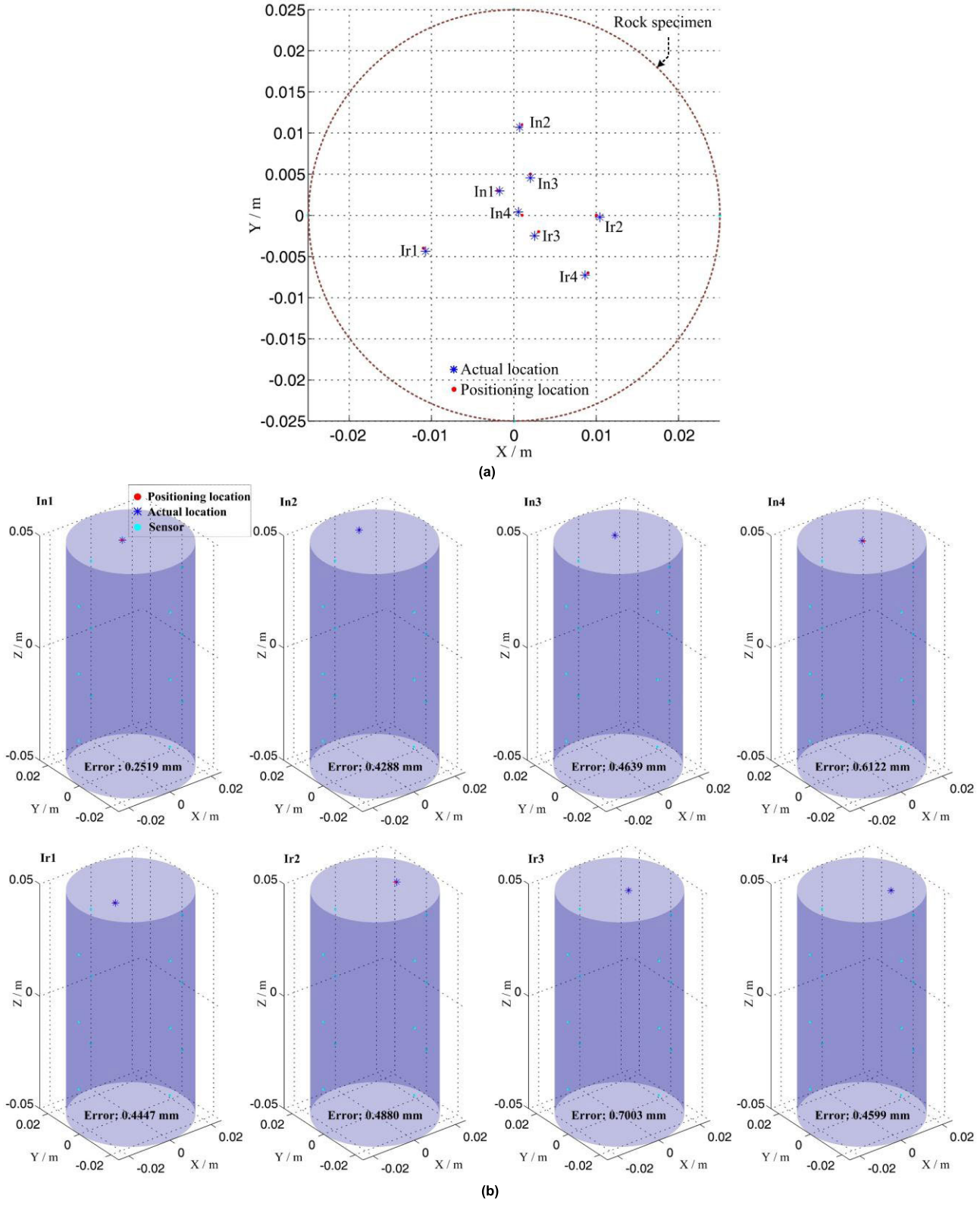

FIGURE 11. Spatial location redetermination of simulated AE events. (a) Top view; (b) 3D view.

for improving the positioning accuracy of AE sources. In applications, it is necessary to suppress the noise and improve the signal quality so that the first arrival signal can be more accurately picked and that the positioning accuracy and reliability of the AE focal points can be further improved.

TABLE 8. The maximum and minimum positioning error and their percentage reduction of the different deviations of first arrivals (type of first arrival: take-off point).

AE events		In1	In2	In3	In4	Ir1	Ir2	Ir3	Ir4
Positioning error (mm)	Max. error (mm)	9.7987	13.5779	11.796	9.3292	6.1194	11.2036	7.7334	9.9652
	Min. error (mm)	5.8131	9.3851	7.7465	3.1739	2.1692	7.0550	2.261	1.0848
	Percentage reduction (%)	41	31	34	66	65	37	71	89

TABLE 9. Comparisons of the positioning errors of initial condition and recalculation.

Seismic source	In1	In2	In3	In4	Ir1	Ir2	Ir3	Ir4
Initial error (mm)	6.0344	12.6706	9.0729	3.1739	5.2128	7.055	2.2617	1.0848
Recalculation error (mm)	0.2519	0.4288	0.4639	0.6122	0.4447	0.488	0.7003	0.4599
Reduced value of error (mm)	5.7825	12.2418	8.609	2.5617	4.7681	6.567	1.5614	0.6249
Percentage reduction of error (%)	95.83	96.62	94.89	80.71	91.47	93.08	69.04	57.61

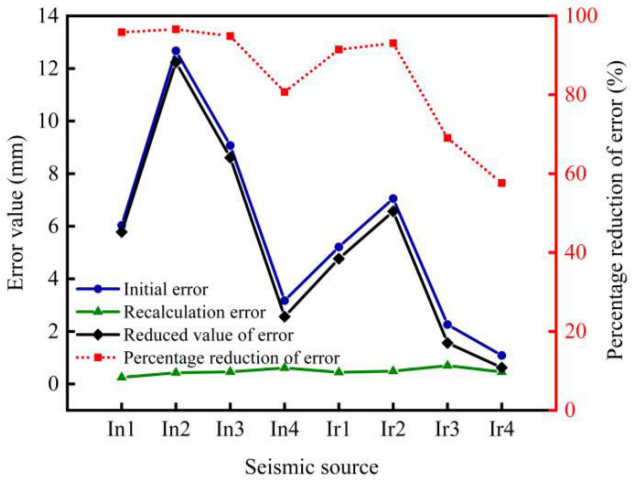

FIGURE 12. The positioning error changes for the initial condition and recalculation for different seismic sources.

C. POSITIONING RECALCULATION RESULTS OF AE EVENTS

Based on the optimization and fine adjustment of the magnitude of the above influencing factors, under the condition that the spatial layout of the sensors remains the same, the positioning locations of the simulated AE events are repositioned, and the results are given in Fig. 11. All the positioning errors of these simulated AE events decrease greatly. It is found that all the positioning errors are less than 1 mm, which can meet the test requirements of the standard cylindrical rock specimen. The minimum and maximum errors are only 0.2519 mm and 0.7003 mm, respectively (the applied minimum grid scale is 1 mm). The calculated locations are extremely close to the actual impact points. This accuracy is much higher than those of other AE source location studies on rock materials, and the location error of previous studies usually reaches more than 10 mm for events inside the sensor array [31], [32].

Comparisons of the positioning errors of the initial condition and recalculation for different seismic sources are shown in Table 9 and Fig. 12. The maximum reduction in the positioning error reaches 12.2418 mm, which is a reduction of 96.62% (In2). The minimum reduction in the positioning error reaches 0.6249 mm, which is a reduction of 57.61% (Ir4). Therefore, the accurate positioning of the passive seismic source is realized by adjusting the number and spatial layout of the sensors and improving the picking accuracy of the first arrival of the signal.

In general, the number and spatial layout of the sensors involved in the positioning calculation have a direct impact on the AE positioning accuracy. As the number of sensors increases, the seismic positioning error tends to decrease gradually. A higher positioning accuracy is achieved if the spatial distribution of the sensors is more uniform. Currently, many passive seismic positioning algorithms are derived based on the modeling of a homogeneous medium. However, the structure of a medium is extremely complex and anisotropic in real situations. Energy absorption is intense, and the wave velocity decreases along some propagation paths. Due to the influence of an abnormal structure, the recorded first arrival signals are always different, even though there is no difference among the radial distances of the wave channels. Therefore, to improve the positioning accuracy and reliability of the passive seismic source, specific analysis and determination are necessary for the channels used according to the quality of the available signals. The use of more sensors in positioning does not always lead to better accuracy. On the premise that infinite channels are available, it is recommended to remove channels with large anomalous forms so that interference is avoided. The reliability of the positioning results tends to improve when signal channels with earlier first arrival are applied. This indicates that the location of the passive seismic source is relatively close to the measuring point and that the homogeneity of the medium along the wave propagation path is relatively higher than that for longer paths. Meanwhile, the sensors involved in positioning calculation can be multiplied and combined to obtain different positioning results. An optimal source location is then obtained through mutual verification.

V. CONCLUSION

1. Once the number of sensors involved in the positioning calculation increases, the maximum and average

values of the positioning errors gradually decrease, and the positioning accuracy generally increases. As the number of sensors ranges from four to twelve, the maximum positioning error changes from 100.472 mm to 12.641 mm, which is a reduction of 60%, and the average positioning error changes from 24.328 mm to 12.641 mm, which is a reduction of 48%.

2. When the number of sensors ranges from four to nine, the minimum positioning error remains at 0.429 mm, and the minimum positioning error reaches 12.641 mm, which is 30 times greater, when the number of sensors increases to twelve. Hence, a better result is achieved when the number of sensors involved in the positioning calculation is nine, accounting for three-fourths of the total number of monitoring sensors used. Under this condition, both the minimum positioning error and the error dispersion are sufficiently low, and the reliability of the positioning results is greatly improved.
3. The positioning accuracy of the AE source is closely related to the types of and deviations in the first arrival signals. Considering the different types, the greatest reduction percentage from the maximum error to minimum error reaches 73% for the same AE event (case Ir4), and the smallest reduction percentage reaches 32% (case In3). On the other hand, with the different deviations, the greatest reduction from the maximum error to minimum error percentage reaches 89% for the same AE event (case Ir4), and the smallest reduction percentage is 32% (case In2).
4. The accurate positioning of an AE event is realized by adjusting the number of sensors and improving the picking accuracy of the first arrival of the signal. The maximum reduction in the positioning error reaches 12.2418 mm, a reduction of 96.62% (In2), and the minimum reduction in the positioning error reaches 0.6249 mm, a reduction of 57.61% (Ir4). Hence, the positioning error decreases significantly.

REFERENCES

[1] L. Dong, D. Sun, X. Li, and K. Du, "Theoretical and experimental studies of localization methodology for AE and microseismic sources without pre-measured wave velocity in mines," *IEEE Access*, vol. 5, pp. 16818–16828, 2017, doi: 10.1109/ACCESS.2017.2743115.

[2] S. Granger, A. Loukili, G. Pijaudier-Cabot, and G. Chanvillard, "Experimental characterization of the self-healing of cracks in an ultra high performance cementitious material: Mechanical tests and acoustic emission analysis," *Cement Concrete Res.*, vol. 37, no. 4, pp. 519–527, Apr. 2007, doi: 10.1016/j.cemconres.2006.12.005.

[3] H. M. Matt and F. L. D. Scalea, "Macro-fiber composite piezoelectric rosettes for acoustic source location in complex structures," *Smart Mater. Struct.*, vol. 16, no. 4, pp. 1489–1499, Aug. 2007, doi: 10.1088/0964-1726/16/4/064.

[4] S. Degala, P. Rizzo, K. Ramanathan, and K. A. Harries, "Acoustic emission monitoring of CFRP reinforced concrete slabs," *Construction Building Mater.*, vol. 23, no. 5, pp. 2016–2026, May 2009, doi: 10.1016/j.conbuildmat.2008.08.026.

[5] A. Carpinteri, J. Xu, G. Lacidogna, and A. Manuello, "Reliable onset time determination and source location of acoustic emissions in concrete structures," *Cement Concrete Compos.*, vol. 34, no. 4, pp. 529–537, Apr. 2012, doi: 10.1016/j.cemconcomp.2011.11.013.

[6] T. Roberts and M. Talebzadeh, "Acoustic emission monitoring of fatigue crack propagation," *J. Constr. Steel Res.*, vol. 59, no. 6, pp. 427–434, Jun. 2003, doi: 10.1016/S0143-974X(02)00064-0.

[7] J. D. Butterfield, A. Krynkin, R. P. Collins, and S. B. M. Beck, "Experimental investigation into vibro-acoustic emission signal processing techniques to quantify leak flow rate in plastic water distribution pipes," *Appl. Acoust.*, vol. 119, pp. 146–155, Apr. 2017, doi: 10.1016/j.apacoust.2017.01.002.

[8] L. E. Rewerts, R. R. Roberts, and M. A. Clark, "Dispersion compensation in acoustic emission pipeline leak location," *Rev. Prog. Quantum Nondestr. Eval.*, vol. 16, pp. 427–434, 1997, doi: 10.1007/978-1-4615-5947-4_57.

[9] S. R. Carlson and R. P. Young, "Acoustic emission and ultrasonic velocity study of excavation-induced microcrack damage at the underground research laboratory," *Int. J. Rock Mech. Min. Sci. Geomech. Abstr.*, vol. 30, no. 7, pp. 901–907, Dec. 1993, doi: 10.1016/0148-9062(93)90042-C.

[10] D. Ozevin and J. Harding, "Novel leak localization in pressurized pipeline networks using acoustic emission and geometric connectivity," *Int. J. Pressure Vessels Piping*, vol. 92, pp. 63–69, Apr. 2012, doi: 10.1016/j.ijpvp.2012.01.001.

[11] A. Nair and C. S. Cai, "Acoustic emission monitoring of bridges: Review and case studies," *Eng. Struct.*, vol. 32, no. 6, pp. 1704–1714, Jun. 2010, doi: 10.1016/j.engstruct.2010.02.020.

[12] D. Aljets, A. Chong, S. Wilcox, and K. Holford, "Acoustic emission source location on large plate-like structures using a local triangular sensor array," *Mech. Syst. Signal Process.*, vol. 30, pp. 91–102, Jul. 2012, doi: 10.1016/j.ymssp.2012.01.012.

[13] A. K. Maji, D. Satpathi, and T. Kratochvil, "Acoustic emission source location using lamb wave modes," *J. Eng. Mech.*, vol. 123, no. 2, pp. 154–161, Feb. 1997, doi: 10.1061/(ASCE)0733-9399(1997)123:2(154).

[14] V. Salinas, Y. Vargas, J. Ruzzante, and L. Gaete, "Localization algorithm for acoustic emission," *Phys. Procedia*, vol. 3, no. 1, pp. 863–871, Jan. 2010, doi: 10.1016/j.phpro.2010.01.111.

[15] J. Fortin, S. Stanchits, G. Dresen, and Y. Guéguen, "Acoustic emission and velocities associated with the formation of compaction bands in sandstone," *J. Geophys. Res-Sol. Ea.*, vol. 111, no. 10, Oct. 2006, Art. no. B10203, doi: 10.1029/2005JB003854.

[16] T. Schumacher, D. Straub, and C. Higgins, "Toward a probabilistic acoustic emission source location algorithm: A Bayesian approach," *J. Sound Vib.*, vol. 331, no. 19, pp. 4233–4245, Sep. 2012, doi: 10.1016/j.jsv.2012.04.028.

[17] F. Ciampa and M. Meo, "A new algorithm for acoustic emission localization and flexural group velocity determination in anisotropic structures," *Compos. A, Appl. Sci. Manuf.*, vol. 41, no. 12, pp. 1777–1786, Dec. 2010, doi: 10.1016/j.compositesa.2010.08.013.

[18] H. Wang and M. Ge, "Acoustic emission/microseismic source location analysis for a limestone mine exhibiting high horizontal stresses," *Int. J. Rock Mech. Mining Sci.*, vol. 45, no. 5, pp. 720–728, Jul. 2008, doi: 10.1016/j.ijrmms.2007.08.009.

[19] K. Nagano, H. Niitsuma, and N. Chubachi, "Automatic algorithm for triaxial hodogram source location in downhole acoustic emission measurement," *Grophysics*, vol. 54, no. 4, pp. 508–513, Apr. 1989, doi: 10.1190/1.1442677.

[20] E. Dehghan Niri and S. Salamone, "A probabilistic framework for acoustic emission source localization in plate-like structures," *Smart Mater. Struct.*, vol. 21, no. 3, Mar. 2012, Art. no. 35009, doi: 10.1155/2013/30748910.1088/0964-1726/21/3/035009.

[21] M. G. Baxter, R. Pullin, K. M. Holford, and S. L. Evans, "Delta t source location for acoustic emission," *Mech. Syst. Signal Process.*, vol. 21, no. 3, pp. 1512–1520, Apr. 2007, doi: 10.1016/j.ymssp.2006.05.003.

[22] S. Xu, J. P. Liu, S. D. Xu, J. Wei, W. B. Huang, and L. B. Dong, "Experimental studies on pillar failure characteristics based on acoustic emission location technique," *T. Nonferr. Metal. Soc.*, vol. 22, no. 11, pp. 2792–2798, Nov. 2012, doi: 10.1016/S1003-6326(11)61534-3.

[23] F. Ciampa and M. Meo, "Acoustic emission source localization and velocity determination of the fundamental mode A0 using wavelet analysis and a Newton-based optimization technique," *Smart Mater. Struct.*, vol. 19, no. 4, Apr. 2010, Art. no. 45027, doi: 10.1088/0964-1726/19/4/045027.

[24] P. Kundu, N. K. Kishore, and A. K. Sinha, "A non-iterative partial discharge source location method for transformers employing acoustic emission techniques," *Appl. Acoust.*, vol. 70, no. 11, pp. 1378–1383, Dec. 2009, doi: 10.1016/j.apacoust.2009.07.001.

[25] J. Hensman, R. Mills, S. G. Pierce, K. Worden, and M. Eaton, "Locating acoustic emission sources in complex structures using Gaussian processes," *Mech. Syst. Signal Process.*, vol. 24, no. 1, pp. 211–223, Jan. 2010, doi: 10.1016/j.ymssp.2009.05.018.
[26] M. J. Eaton, R. Pullin, and K. M. Holford, "Acoustic emission source location in composite materials using delta t mapping," *Compos. A, Appl. Sci. Manuf.*, vol. 43, no. 6, pp. 856–863, Jun. 2012, doi: 10.1016/j.compositesa.2012.01.023.
[27] M. Ohtsu, "Simplified moment tensor analysis and unified decomposition of acoustic emission source: Application to *in situ* hydrofracturing test," *J. Geophys. Res., Solid Earth*, vol. 96, no. B4, pp. 6211–6221, Apr. 1991, doi: 10.1029/90JB02689.
[28] P. M. Eleftherion, "Partial discharge. XXI. acoustic emission based PD source location in transformers," *IEEE Elect. Insul. Mag.*, vol. 11, no. 6, pp. 22–26, Nov. 1995, doi: 10.1109/57.475905.
[29] L. Dong and X. Li, "A Microseismic/Acoustic emission source location method using arrival times of PS waves for unknown velocity system," *Int. J. Distrib. Sensor Netw.*, vol. 9, no. 10, Oct. 2013, Art. no. 307489, doi: 10.1155/2013/307489.
[30] T. Q. Jiang and S. J. Pei, "Micro-seismic event location based on Newton iteration method and grid-search method," *J. Min. Sci. Technol.*, vol. 4, no. 6, pp. 480–488, Dec. 2019, doi: 10.19606/j.cnki.jmst.2019.06.002.
[31] L. J. Dong, X. B. Li, Z. L. Zhou, G. H. Chen, and M. A. Ju, "Three-dimensional analytical solution of acoustic emission source location for cuboid monitoring network without pre-measured wave velocity," *T. Nonferr. Metal. Soc.*, vol. 25, no. 1, pp. 293–302, Feb. 2015, doi: 10.1016/S1003-6326(15)63604-4.
[32] W. Mao, S. Aoyama, and I. Towhata, "A study on particle breakage behavior during pile penetration process using acoustic emission source location," *Geosci. Frontiers*, vol. 11, no. 2, pp. 413–427, Mar. 2020.

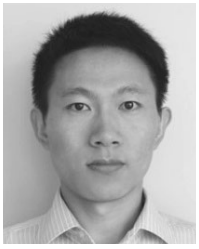

YANLONG CHEN was born in Chengde, Hebei, China, in 1982. He received the B.S. and M.S. degrees in mining engineering from the China University of Mining and Technology, Xuzhou, Jiangsu, China, in 2007 and 2010, respectively, and the Ph.D. degree in earth resources from the School of Engineering, Kyushu University, Fukuoka, Japan, in 2013.

From 2014 to 2017, he was a Lecturer, and since 2018, he has been an Associate Professor with the State Key Laboratory for Geomechanics and Deep Underground Engineering, China University of Mining and Technology. He is mainly involved in the study of mechanics and engineering of mining rock mass and slope stability.

MINGWEI ZHANG was born in Changle, Shandong, China, in 1984. He received the B.S. and M.S. degrees in mining engineering from the China University of Mining and Technology, Xuzhou, Jiangsu, China, in 2008 and 2011, respectively, and the Ph.D. degree in mining engineering from Kyushu University, Fukuoka, Japan, in 2014.

From 2014 to 2018, he was a Lecturer, and since 2019, he has been an Associate Professor with the State Key Laboratory for Geomechanics and Deep Underground Engineering, China University of Mining and Technology. He is mainly involved in the study of geotechnical engineering investigation, microseismic and acoustic emission, and nondestructive testing of road and bridge pile foundations.

HAOSHUAI WU was born in Yiwu, Zhejiang, China, in 1990. He received the B.S. degree in engineering mechanics and the M.S. degree in general mechanics and mechanics foundation from the School of Mechanics and Civil Engineering, China University of Mining and Technology, Xuzhou, Jiangsu, China, in 2014 and 2018, respectively, where he is currently pursuing the Ph.D. degree in geotechnical engineering. His main research topics include rock dynamics and the damage characteristics of rock material.

KAI ZHANG was born in Zhoukou, Yancheng, Henan, China, in 1984. He received the B.S. degree in engineering mechanics from the China University of Mining and Technology, in 2005, and the Ph.D. degree in rock mechanics from the Institute of Rock and Soil Mechanics, Chinese Academy of Sciences, in 2010.

He is currently a Professor and the Doctoral Supervisor with the China University of Mining and Technology. He is mainly involved in the study of geomechanics and underground engineering.

DEYU QIAN was born in Fengyang, Anhui, China, in 1987. He received the B.S. degree in mining engineering from the Anhui University of Science and Technology, Huainan, China, in 2008, the M.S. degree in mining engineering from the China University of Mining and Technology, Xuzhou, Jiangsu, China, in 2011, and the Ph.D. degree in earth resources from the School of Engineering, Kyushu University, Fukuoka, Japan, in 2016.

Since 2019, he has been an Associate Professor with the School of Mines, China University of Mining and Technology. He is mainly involved in teaching and scientific research in pipe jacking, soft rock engineering, grouting engineering, underground space engineering, tunnel surrounding rock control, rock mechanics and strata control, volcano and geothermal systems, geothermal resource development, earth resources, and mining engineering.